IEEE Access
Multidisciplinary | Rapid Review | Open Access Journal

Date of publication xxxx 00, 0000, date of current version xxxx 00, 0000.

Digital Object Identifier 10.1109/ACCESS.2017.DOI

A Novel Non-Invasive Estimation of Respiration Rate from Motion Corrupted Photoplethysmograph Signal Using Machine Learning Model

MD NAZMUL ISLAM SHUZAN[1], MOAJJEM HOSSAIN CHOWDHURY[2], MD SHAFAYET HOSSAIN[3], MUHAMMAD E.H. CHOWDHURY[2], (SENIOR MEMBER, IEEE), MAMUN BIN IBNE REAZ[3], (SENIOR MEMBER, IEEE), M. MONIR UDDIN[4], AMITH KHANDAKAR[2] , (SENIOR MEMBER, IEEE), ZAID B. MAHBUB[4], AND SAWAL HAMID MD ALI.[3]

[1]Department of Electrical and Computer Engineering, North South University, Dhaka 1229, Bangladesh (e-mail: nazmul.shuzan@northsouth.edu)
[2]Department of Electrical Engineering, Qatar University, Doha 2713, Qatar (e-mail: moajjem.c@qu.edu.qa, mchowdhury@qu.edu.qa, amitk@qu.edu.qa)
[3]Department of Electrical, Electronic and System Engineering, Universiti Kebangsaan Malaysia, Bangi 43600, Selangor, Malaysia, Qatar (e-mail: p108100@siswa.ukm.edu.my, mamun@ukm.edu.my, sawal@ukm.edu.my)
[4]Department of Mathematics and Physics, North south University, Dhaka-1229, Bangladesh (e-mail: monir.uddin@northsouth.edu, zaid.mahbub@northsouth.edu)

Corresponding author: Muhammad E.H. Chowdhury (e-mail: mchowdhury@qu.edu.qa), Mamun bin Ibne Reaz (mamun@ukm.edu.my), Shafayet Hossain (p108100@siswa.ukm.edu.my).

This work was made possible by NPRP12S-0227-190164 from the Qatar National Research Fund, a member of Qatar Foundation, Doha, Qatar. Open Access funding provided by the Qatar National Library"

ABSTRACT Respiratory ailments such as asthma, chronic obstructive pulmonary disease (COPD), pneumonia, and lung cancer are life-threatening. Respiration rate (RR) is a vital indicator of the wellness of a patient. Continuous monitoring of RR can provide early indication and thereby save lives. However, a real-time continuous RR monitoring facility is only available at the intensive care unit (ICU) due to the size and cost of the equipment. Recent researches have proposed Photoplethysmogram (PPG) and/ Electrocardiogram (ECG) signals for RR estimation however, the usage of ECG is limited due to the unavailability of it in wearable devices. Due to the advent of wearable smartwatches with built-in PPG sensors, it is now being considered for continuous monitoring of RR. This paper describes a novel approach for RR estimation using motion artifact correction and machine learning (ML) models with the PPG signal features. Feature selection algorithms were used to reduce computational complexity and the chance of overfitting. The best ML model and the best feature selection algorithm combination was fine-tuned to optimize its performance using hyperparameter optimization. Gaussian Process Regression (GPR) with Fit a Gaussian process regression model (Fitrgp) feature selection algorithm outperformed all other combinations and exhibits a root mean squared error (RMSE), mean absolute error (MAE), and two-standard deviation (2SD) of 2.63, 1.97, and 5.25 breaths per minute, respectively. Patients would be able to track RR at a lower cost and with less inconvenience if RR can be extracted efficiently and reliably from the PPG signal.

INDEX TERMS Photoplethysmogram, Respiration Rate, Machine Learning, Feature Selection, Motion Artifact Correction, Gaussian Process Regression

I. INTRODUCTION

ONE of the most important physiological parameters that are used to diagnose abnormality in a human body is respiration rate (RR). It is one of the four primary vital signs along with heart rate, blood pressure, and body temperature. RR is expressed as the number of breaths a person takes in one minute (breaths/minute). An unusual RR is often a cause for concern and is often used as an indicator for an ailing body [1]–[3]. Hence, it is a vital parameter that is monitored by healthcare personnel when they check for acute deterioration of the patients [4]. Problems in the respiratory system [5], cardiac arrest [6] and even death occurring during

This article has been accepted for publication in a future issue of this journal, but has not been fully edited. Content may change prior to final publication. Citation information: DOI 10.1109/ACCESS.2021.3095380, IEEE Access

hospital stay [7] can be predicted by an increased RR. So, hospital patients who are very ill have their RR measured every few hours [8]. Its importance is also noted in emergency departments of hospitals where they use RR for screening [9]. Furthermore, RR is used to diagnose pneumonia [10], [11]and sepsis during primary treatment.

RR is also used to identify pulmonary embolism [12], [13] and hypercarbia [14]. Hence, there must be an accurate way of measuring RR in clinical settings as it would greatly benefit both the patient and health care providers. However, even now it is mostly being estimated by counting the breaths manually. This method is not suitable when the patient needs to be monitored unobtrusively. It also requires more effort from the medical personnel when measuring RR. Furthermore, this method is error-prone [15], [16] and the other is capnography, where the concentration of partial pressure of carbon dioxide (CO2) in the respiratory gases [17] is measured. It is one of the most accurate ways of measuring RR. However, it is cumbersome to use. As a result, it is mainly used during anesthesia and intensive care. So, alternate noninvasive methods need to be developed.

One of the most popular alternatives is to use either electrocardiogram (ECG) or photoplethysmogram (PPG) to estimate RR. ECG and PPG signals are easily measured during a clinical assessment. They can also be measured easily by devices for health care monitoring. Hence, there is a potential for automating the process of RR estimation without the necessity of using capnography machines. Many algorithms have been proposed for estimating RR from ECG [18]–[20]. However, it has been observed that respiratory signals extracted from ECG appeared flat in ICU patients even though they were breathing sufficiently [21]. Besides, the clinical ECG system still requires trained professionals to operate and are bulky. Hence, the PPG signal has become more appealing for estimating RR.

Several recent developments on the estimation methods of the RR were comprehensively summarized in this section [22]–[24]. A diverse range of methodologies was used to test the efficiency of RR algorithms using ECG and PPG waveform and the majority of them used PPG signals. Various issues make it difficult to reinvestigate the performance of the reported algorithms. In [23], [24], about 100 algorithms have been suggested to measure the respiratory rate (RR) from ECG and PPG. All high-performance algorithms are composed of innovative variations of time domain RR estimation and modulation fusion techniques. In [10], the authors proposed a novel method for estimating the respiratory rate in real-time from the PPG signals. The incremental-merge segmentation algorithm was used to derive three respiratory-induced variations (frequency, strength, and amplitude) from the PPG signal. The smart fusion showed trends of improved estimation of root mean square error (RMSE) 3.0 breaths per min (bpm) compared to the individual estimation methods.

In [25], the authors introduced a feasible alternative for estimating child respiratory rates during evaluation in the emergency department, particularly if the segments of PPG contaminated by the movement artifacts were automatically discarded by an appropriate algorithm. They achieved a mean absolute error (MAE) of 5.2 bpm for the age group of 5-12 years. In [26], a novel method was proposed to estimate the RR of the PPG signal using joint sparse signal reconstruction (JSSR) and spectra fusion (SF). In [27], a smart fusion method was introduced based on ensemble empirical mode decomposition (EEMD) to improve RR extraction from PPG. In [28], they applied EEMD and tested on two different datasets. In [29], PPG-RR calculations were retrospectively conducted on PPG waveforms derived from the data warehouse and compared with RR reference values during the validation stage of the algorithm. In [30], the use of amplitude fluctuations of the transmittance mode finger PPG signal in RR estimation by comparing four time-frequency (TF) signal representation approaches cascaded with a particle filter was studied.

In [31], a case study of 10 patients was reported for whom fewer RR estimates were derived from PPG signals relative to accelerometry. In [32], the disparity in the precision of PPG-derived respiration frequency between measurements at various body sites for normal and deep breathing conditions was investigated. Respiratory signals were derived from PPG signals of 36 healthy subjects using the frequency demodulation method to measure respiration frequency via spectral power density. The linearity between the PPG-derived and the reference respiratory frequency was highest on the forehead. In [33], Charlton's method [23], [24] was used with remote PPG (rPPG) based signals to boost the accuracy of the respiration rate estimation. Few improvements have been made to make it usable for rPPG signals. Using PPG-contact algorithms on remote PPG signals can lead to respiratory rate estimates with an MAE of less than 3 bpm and the reported MAE and RMSE Of 3.03 and 3.69 bpm, respectively.

Table 1,summarizes a wide variety of RR estimation algorithms from the PPG that have been published in recent years. None of them used machine learning (ML) models to estimate the RR from ECG or PPG and their fusion. Therefore. There is a potential scope to use ML models to improve the RR estimation algorithm. With the increase of the availability of annotated datasets, it is possible to use ML techniques in RR algorithms [22], which is a major motivation of this study. However, to the best of our knowledge, no recent work has derived t- domain, f-domain, and statistical features from PPG signal to estimate reliably RR using the machine learning models. However, in real-world PPG signal is often corrupted with the motion artifact and it is therefore important to remove motion artifact from the PPG signals so that feature extraction can be done on complete dataset to estimate the respiration rate (RR) from even motion corrupted PPG signals. In our previous studies [34]–[36], several time-domain features were calculated from the original signal and its derivatives. Several features were extracted for RR estimation from the PPG signal in this study, which was not used before by any other research group.

This manuscript is divided into four sections where **Sec-**

This article has been accepted for publication in a future issue of this journal, but has not been fully edited. Content may change prior to final publication. Citation information: DOI 10.1109/ACCESS.2021.3095380, IEEE Access

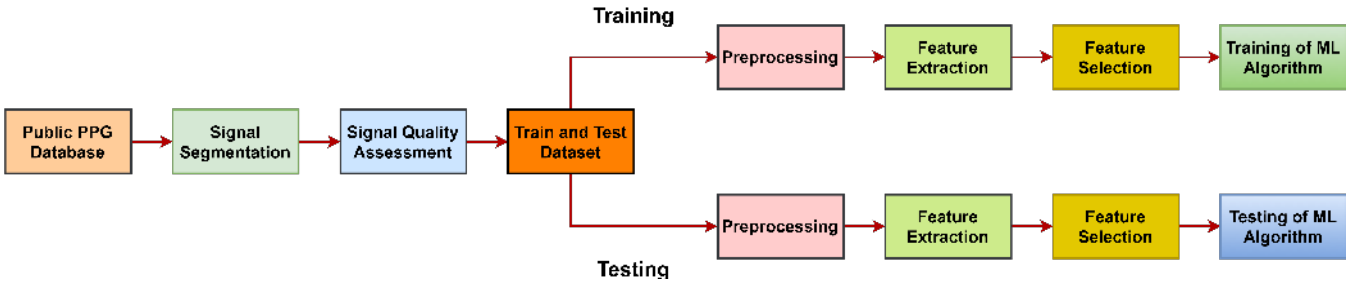

FIGURE 1: Overview of the process

tion I addresses the fundamentals of the PPG signal, the associated works, and the motivation for this study. The database description, pre-processing, evaluation measures, and methodology are discussed in **Section II** while **Section III** outlines the results and discusses them, and compares them with some other research solutions, while, while **Section V** concludes the work.

TABLE 1: Summary of methods for respiration rate estimation

Author	Method Used
Karlen et al. [10]	Fast Fourier Transformation (FFT)
Orphanidou et al. [19]	Ensemble Empirical Mode Decomposition
Pimentel et al. [12], [37]	Auto-regressive Model
Philip et al. [16]	Spot Assessment
Mirmohamadsadegh et al. [20]	Instantaneous Frequency Tracking Algorithm
Lin et al. [38]	Wavelet-Based Algorithm
Fleming et al. [39]	Auto-regressive Model
Zhou et al. [40]	Independent Component Analysis (ICA) Algorithm
Moreno et al. [41]	Digital Filtering
Nilsson et al. [42]	Digital Filtering
Motin et al. [27], [28]	Empirical Mode Decomposition
Jarchi et al. [31]	Accelerometer Based
Hartmann et al. [32]	Fast Fourier Transformation (FFT)
Pirhonen et al. [30]	Wavelet-Based
Zhang et al. [26], [43]	Joint Sparse Signal Reconstruction
Madhav et al. [44]	Modified multi scale principal component analysis (MMSPCA)

II. METHODOLOGY

This section summarizes the dataset description and the pre-processing techniques, various features that were extracted, different feature selection algorithms, and the different machine learning models that were implemented for RR estimation in this study.

Figure 1 shows the overall methodology where PPG signal from the publicly available VORTAL dataset [23], [24] is first segmented into windows of 32 seconds. The PPG signals are then split into 80% training and 20% test sets, respectively for 5-fold cross-validation. Firstly, the segmented PPG signals were filtered and the motion artifacts were removed from the PPG signals . Then their meaningful features were extracted and feature selection algorithms were used to reduce feature dimensions to avoid the risk of overfitting and to reduce the computation time. The selected features were used to train, validate and test machine learning models. An unseen 20% test-set per fold was used to predict the RR value from the PPG features.

TABLE 2: Characteristics of the subjects in Vortal Dataset

	median	Lower quartile	Upper quartile
Sex (female)	54%	-	-
Age (years)	29	26	32
BMI ((kg/m^2))	23	21	26
Respiration Rate (bpm)	5-32	-	-

A. DATASET DESCRIPTION

Electrocardiogram (ECG) and photoplethysmogram (PPG) signals and the respiration rate (RR) from 39 subjects are available in the VORTAL dataset. The PPG signals used were acquired during the resting period and sampled at 500Hz sampling frequency. The summary of the dataset is shown in **Table 2**.

The signals were segmented into windows of 32 seconds as it allows a sufficient amount of breaths to take place so that RR can be calculated reliably [10], [23], [24]. A shorter window will pose a problem to the respiration rate while the longer window will not be practically feasible. 758 PPG segments of 32-seconds were obtained.

B. PREPROCESSING

The PPG waveform in the dataset has motion artifact and high-frequency noise components. These noises can hamper the feature extraction process. Therefore, to remove the high-frequency noises, the PPG waveforms were filtered through a low-pass Butterworth Infinite Impulse Response (IIR) Zero-Phase Filter [45]. **Figure 2** shows the motion-artifact free raw PPG signal with high-frequency noise overlaid with the filtered signal. A sixth-order IIR filter with a cut-off frequency of 25 Hz was implemented in MATLAB.

In real-world PPG data acquisition, one common problem with the PPG signals is that it is often become corrupted by the motion artifact (MA). MA causes spikes and other distortion to occur in the signal. This makes it very difficult to extract meaningful time-domain features. Several signal processing methods have been used for removing motion artifacts from the one-dimensional signal. Among these recently Variational Mode Decomposition (VMD) was used to remove the motion artifacts from the PPG signals [46], [47]. The quality of the segmented signals was evaluated after filtering and motion artifact correction to reject unfit data, however, none of the segments were found unfit.

This article has been accepted for publication in a future issue of this journal, but has not been fully edited. Content may change prior to final publication. Citation information: DOI 10.1109/ACCESS.2021.3095380, IEEE Access

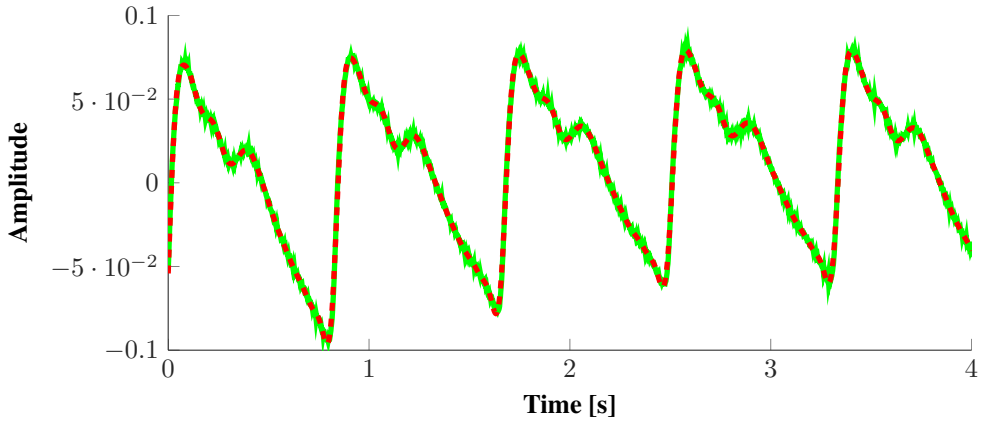

FIGURE 2: Filtered signal overlaid on the raw PPG signal.

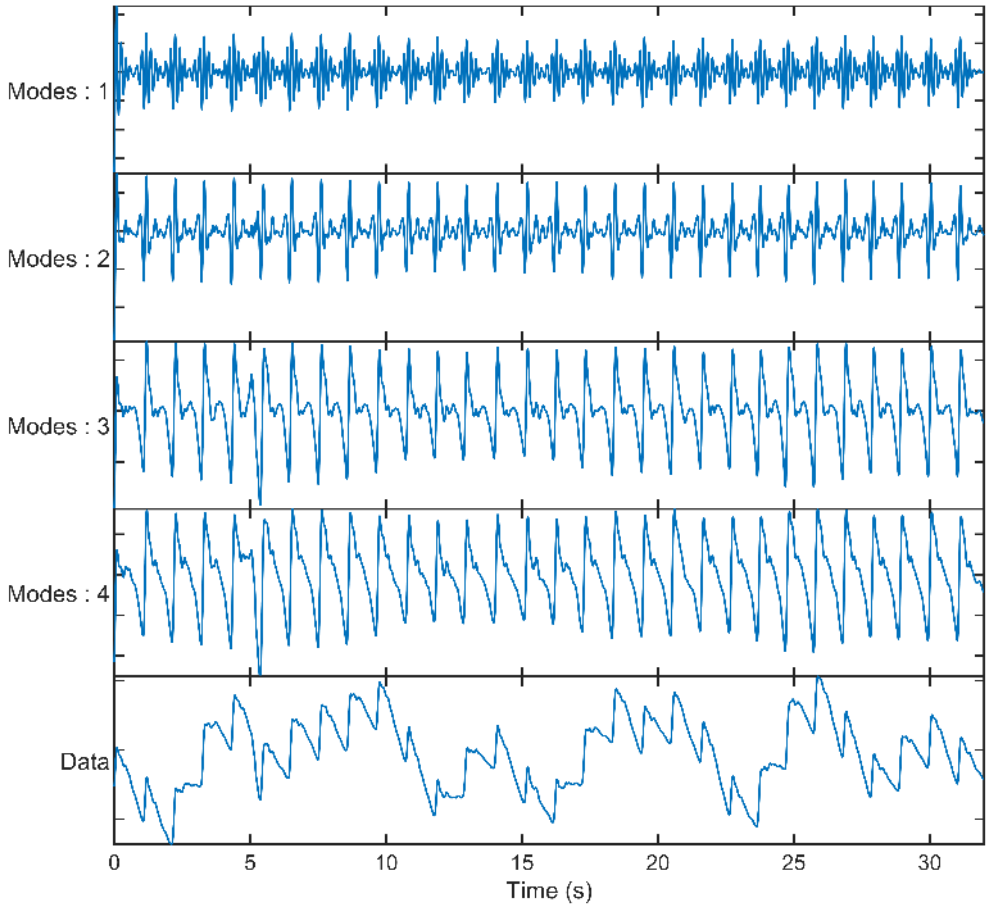

FIGURE 3: Reconstruction of PPG signal using different Modes of VMD used for MA correction.

The following section is briefly introducing the concept of removing motion artifact using VMD technique.

A real valued signal, $(x(t))$ is decomposed into a set of modes(k number of μ_k modes) in VMD. The set of modes, in frequency domain, are called narrowband intrinsic mode functions (IMF). IMF are generated using the following method:

1) Hilbert Transform is used to make the analytic signal
2) The analytic signal is demodulated to baseband tuned to the estimated center frequency
3) L2-norm of the gradient of the signal is used to calculate the bandwidth

The method described above is posed as an optimization

This article has been accepted for publication in a future issue of this journal, but has not been fully edited. Content may change prior to final publication. Citation information: DOI 10.1109/ACCESS.2021.3095380, IEEE Access

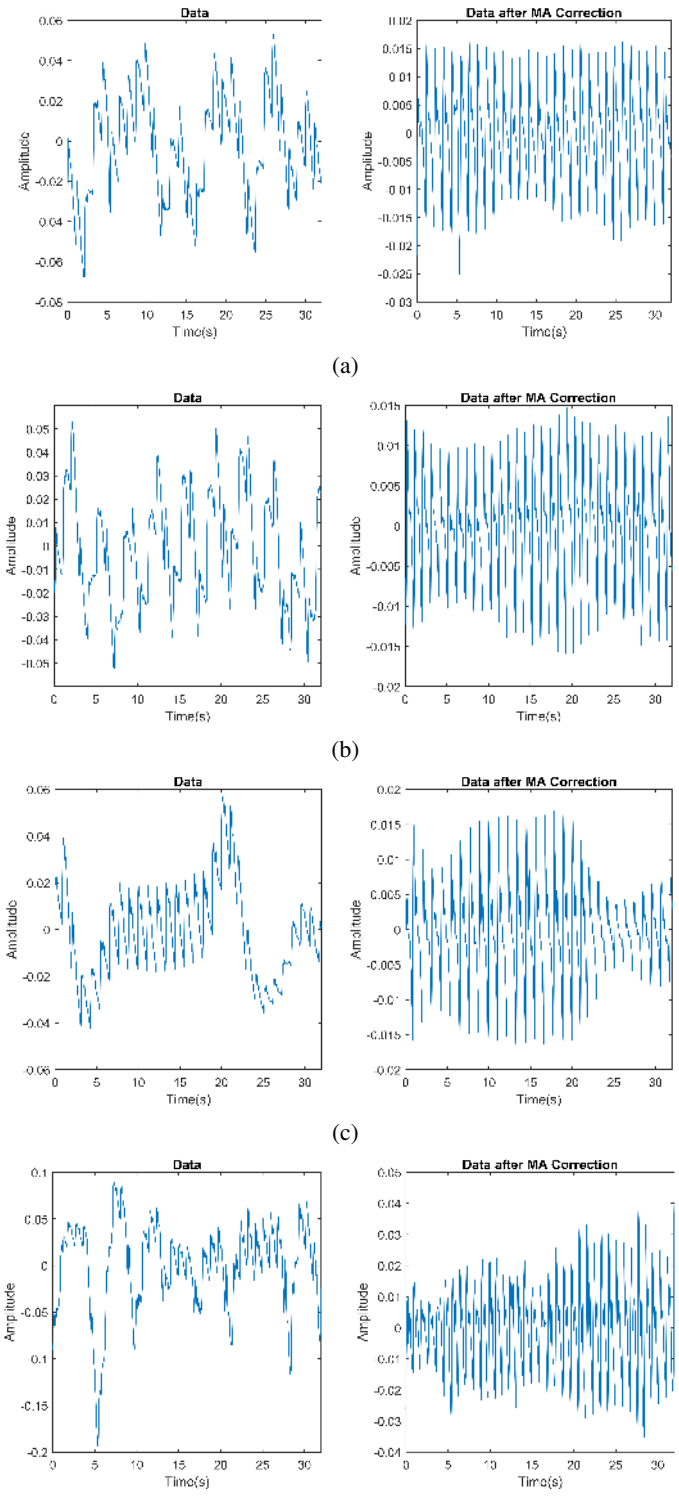

FIGURE 4: Motion Artifact Correction from same motion corrupted PPG signal segments

problem. The aim of which is to minimize the total bandwidth taken by all the modes such that the signal is reconstructed by the modes collectively.

Equation 1 shows the mathematical formulation of the optimization problem where $\{\mu_k\} = \{\mu_1, \cdots, \mu_k\}$ are set of all modes and $\{\omega_k\} = \{\omega_1, \cdots, \omega_k\}$ are its corresponding

This article has been accepted for publication in a future issue of this journal, but has not been fully edited. Content may change prior to final publication. Citation information: DOI 10.1109/ACCESS.2021.3095380, IEEE Access

center frequencies.

$$\min_{\{\omega_k\},\{\mu_k\}} \{\Sigma_k ||\delta_t[(\delta(t) + \frac{j}{\pi t}) * \mu_k(t)]e^{-j\omega_k t}||_2^2\} \quad (1)$$

$$s.t\ \Sigma_k \mu_k = x(t)$$

VMD is robust and can eliminate noise and disturbances. In this work, empirically decided five modes were extracted from the PPG signal. It was observed that the last mode contained most of the motion artifact that corrupts the signal. The PPG signal was reconstructed using the first 4 modes.

In **Figure 3**, reconstructed data is shown. The first row shows signal reconstructed using one mode, the second row shows the signal reconstruction using the first two modes and so on. Adding all five modes gives the original data back with MA. It can be seen that, using the first four modes gives a good reconstruction of the signal with most of the MA corruption removed.

In **Figure 4**, various PPG signals are shown where the MA has been removed from the PPG signals. It can be noticed that PPG signals with very large MA corruption were successfully cleaned by VMD. The IMF modes of the signals are available in the supplementary materials.

C. FEATURE EXTRACTION

Figure 5 summarizes different types of features extracted in this study. PPG waveforms are rich in detail and contain many features of interest. They contain features such as systolic peak, foot of the waveform, pulse width, peak-to-peak interval, etc. To extract the meaningful features, as shown in **Table 3**, we used the feature extraction techniques described in [34].

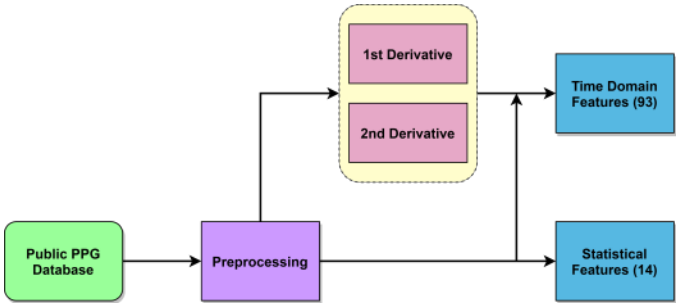

FIGURE 5: Overview of the Feature Extraction method.

The preprocessed signal is used to calculate statistical features while the time-domain features were extracted from the PPG signal and its 1st and 2nd derivatives (in **Figure 6** and **7**) From the derivatives of the signal, the main features were the first peak and first trough of the signal. Time and amplitude features were calculated afterward and summarized in **Table 3** and **4**. Mean, standard deviation, and variance of most of the time-domain features was also calculated. This is because to capture the distortion and modulation caused by breathing on PPG, these features are important. These time-domain features were identified from different previous works [34]–[36]. Statistical features used in this work were identified from [35]. In total, 107 features were extracted to feed the machine learning models.

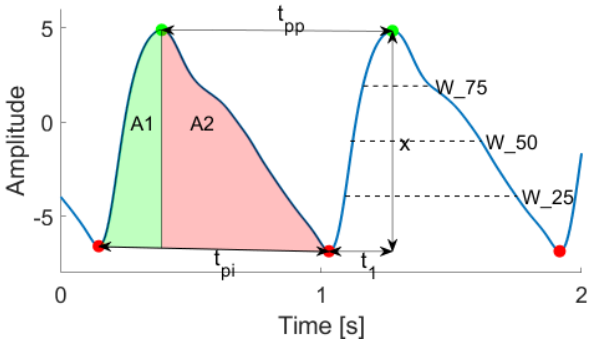

FIGURE 6: PPG signal with some time-domain features.

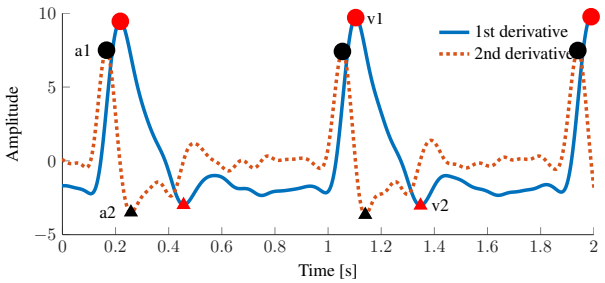

FIGURE 7: 1st and 2nd derivatives of PPG Signal.

D. FEATURE SELECTION

Feature selection decreases the data dimensionality by choosing only a subset of calculated characteristics (predictor variables) to construct a model. Feature selection algorithms (FSA) look for a subset of predictors that optimally model the responses tested, considering the constraints such as feature importance and subset size. The Feature Ranking Library (FSLib) is an often-used MATLAB library [48]. In this work, 10 Feature selection algorithms have been used and after several feature combinations, the best feature ranking technique for this problem is identified.

Fit a Gaussian process regression model (Fitrgp): Fitrgp can find the predictor weights by taking the exponential of the negative learned length scales contained in the kernel information property [49], [50]. In **Table 5**, It is found that the most contributory features are 11, out of 107 features and 5 among the 11 selected features are derived from the derivative of the PPG signal. And 3 statistical and 3 time domain PPG signal features participated equally in top 11 features.

Least absolute shrinkage and selection operator (Lasso): Lasso minimizes the variance of inference by retaining the sum of the absolute values of the model parameters smaller than the fixed value [51]. The most contributory features are 17, out of 107 features where 9 features were

This article has been accepted for publication in a future issue of this journal, but has not been fully edited. Content may change prior to final publication. Citation information: DOI 10.1109/ACCESS.2021.3095380, IEEE Access

TABLE 3: Fifteen time-domain features with their mean, standard deviation and variance

Features	Definition
Systolic Peak	The amplitude of ('sys') from the PPG signal
Height of foot	The amplitude of ('amp foot') from the PPG signal
New Systolic peak	The amplitude of ('x') from the PPG signal
Systolic peak time	The time interval from the foot of the PPG signal to the systolic peak ('t1') pulse
Interval	The time interval from foot to next foot ('tpi')
Peak-to-Peak Interval	The time distance between two consecutive systolic peaks ('tpp')
t1/x	The ratio of systolic peak time to the systolic amplitude of the PPG waveform
t1/tpi	The ratio of systolic peak time to pulse interval of the PPG waveform
x/(tpi-t1)	The ratio of 'x' to the difference between 'tpi'and 't1'
Rising area	Area from first foot to systolic peak('A1')
Decay area	Area from systolic peak to foot('A2')
A1/A2	The ratio from 'A1' to 'A2'
Width (25%)	The width of the PPG signal at 25% amplitude of 'x'
Width (50%)	The width of the PPG signal at 50% amplitude of 'x'
Width (75%)	The width of the PPG signal at 75% amplitude of 'x'

TABLE 4: Sixteen features derived from the first and second derivative with mean, standard deviation, and variance

Features	Definition
v1	The first maximum peak from the 1st derivative of the PPG signal
tv1	The first maximum peak time from the 1st derivative of the PPG signal
v2	The first minimum peak amplitude from the first derivative
tv2	The first minimum peak time from the first derivative of the PPG signal
a1	The first maximum peak amplitude from the 2nd derivative of the PPG signal
ta1	The first maximum peak time from the 2nd derivative of the PPG signal
a2	The first minimum peak amplitude from the second derivative of the PPG signal
ta2	the first minimum time amplitude from the second derivative of the PPG signal
v2/v1	The ratio between v2 and v1
a2/a1	The ratio between a2 and a1
tv1/tv2	The ratio between tv1 and tv2
ta1/ta2	The ratio between ta1 and ta2
tv1/ta1	The ratio between tv1 and ta1
tv1/ta2	The ratio between tv1 and ta2
tv2/ta1	The ratio between tv2 and ta1
tv1/ta1	The ratio between tv1 and ta2

derived from the PPG signal (**Table 5**), where 7 derivative features and 1 statistical also contributed in top 17.

Relieff feature selection (RFS): RFS works much better to approximate the significance of the function for distance-based supervised models that use pairwise distances between the observations to predict [52], [53]. **Table 5**, shows that 27 features are the most contributory features and 16 out of them are PPG signal and 11 features are their derivative.

Feature selection with adaptive structure learning (Fsasl): Fsasl is focused on linear regression and its only limitation is the high computational complexity, which can be expensive for the high-dimensional results [54]. **Table 6**, shows the most contributory 19 features where 9 are the derivative features, 8 are the PPG signal features and only 2 are statistical features.

Unsupervised feature selection with ordinal locality (Ufsol): To implement the selected feature classes, a triplet-based loss function is added to maintain the ordinal localization of original data, which leads to distance-based clustering activities. And then simplify orthogonal base clustering by imposing an orthogonal restriction on the function projection matrix. As a consequence, a general structure for simultaneous collection and clustering of features is addressed [55]. **Table 6**, shows the most contributory 27 features, where 19 are the derivative features, 5 features are from the PPG signal and 3 from statistical features.

Laplacian method (LM): Another unsupervised approach is the LM, where the value of a feature is determined by its capacity to conserve the locality. This approach builds the closest neighbor graph to model the local geometric structure. LS algorithm is searching for features that respect the structure of this graph [56]. **Table 6**, lists the most contributory 25 features where 14 features were extracted from the derivative of the PPG signal and 11 features from the signal.

Unsupervised dependence feature Selection (UDFS): UDFS is a projection-free function selection model based on l2.0-standard equality constraints. UDFS conducts the collection of function subsets by optimizing two terms: one term increases the dependency on the original results, while the other term maximizes the dependence of selected features on cluster labels to direct the phase of subset feature selection [57]. It was found that 11 out of 20 most contributory features were from the PPG signal (**Table 6**) and 6 statistical and 3 derivative features were also participated in the top 20 features.

Infinite Latent feature selection (ILFS): ILFS is a probabilistic approach to latent feature selection that performs the ranking stage by taking into consideration all feasible sub-

This article has been accepted for publication in a future issue of this journal, but has not been fully edited. Content may change prior to final publication. Citation information: DOI 10.1109/ACCESS.2021.3095380, IEEE Access

TABLE 5: Top-ranked features using Fitrgp, Lasso, and Relieff based Feature Selection Algorithms

Algorithm	Best Selected Features		
Fitrgp (11)	47.mean(tv1)	103.iqr(sig)	106. signal_entropy(sig)
	54.mean(v2/v1)	104. skewness(sig)	5.mean(tpi)
	7.mean(t1/x)	53.mean(ta2)	4.mean(t1)
	55.mean(a2/a1)	49.mean(tv2)	
Lasso (17)	46.mean(v1)	9.mean(x/(tpi-t1))	39.var(x/(tpi-t1))
	1.mean(sys amp)	49.mean(tv2)	5.mean(tpi)
	56.mean(tv1/tv2)	44.var(w_50)	14.mean(w_50)
	93.var(tv2/ta2)	16.std(sys amp)	85.var(ta2)
	106.signal_entropy(sig)	27.std(A1/A2)	92.var(tv2/ta1)
	25.std(A1)	86.var(v2/v1)	
Relieff (27)	1.mean(sys amp)	2.mean(foot amp)	4.mean(t1)
	5.mean(tpi)	7.mean(t1/x)	8.mean(t1/tpi)
	12.mean(A1/A2)	13.mean(w_25)	16.std(sys amp)
	17.std(foot amp)	19.std(t1)	20.std(tpi)
	22.std(t1/x)	25.std(A1)	28.std(w_25)
	37.var(t1/x)	47.mean(tv1)	48.mean(v2)
	49.mean(tv2)	51.mean(ta1)	52.mean(a2)
	54.mean(v2/v1)	55.mean(a2/a1)	56.mean(tv1/tv2)
	57.mean(ta1/ta2)	58.mean(tv1/ta1)	59.mean(tv1/ta2)

TABLE 6: Top-ranked features using Fsasl, Ufsol, Laplacian and UDFS based Feature Selection Algorithms

Algorithm	Best Selected Features		
Fsasl(19)	38.var(t1/tpi)	41.var(A2)	40.var(A1)
	36.var(tpp)	105.kurtosis(sig)	75.std(tv1/ta2)
	68.std(a2)	94.maxfreq	86.var(v2/v1)
	48.mean(v2)	84.var(a2)	93.var(tv2/ta2)
	91.var(tv1/ta2)	33.var(x)	39.var(x/(tpi-t1))
	85.var(ta2)	88.var(tv1/tv2)	32.var(amp of foot)
	8.mean(t1/tpi)		
Ufsol (27)	3.mean(x)	11.mean(A2)	10.mean(A1)
	2.mean(foot amp)	1.mean(sys amp)	25.std(A1)
	26.std(A2)	33.var(x)	40.var(A1)
	39.var(x/(tpi-t1))	82.var(a1)	12.mean(A1/A2)
	42.var(A1/A2)	78.var(v1)	9.mean(x/(tpi-t1))
	17.std(amp of foot)	38.var(t1/tpi)	93.var(tv2/ta2)
	99.std(sig)	105.kurtosis(sig)	100.mad(sig)
	79.var(tv1)	80.var(v2)	57.mean(ta1/ta2)
	41.var(A2)	27.std(A1/A2)	106.signal_entropy(sig)
Laplacian(25)	78.var(v1)	66.std(a1)	62.std(v1)
	63.std(tv1)	68.std(a2)	24.std(x/(tpi-t1))
	31.var(sys amp)	36.var(tpp)	73.std(ta1/ta2)
	38.var(t1/tpi)	21.std(tpp)	89.var(ta1/ta2)
	18.std(x)	79.var(tv1)	75.std(tv1/ta2)
	64.std(v2)	35.var(tpi)	23.std(t1/tpi)
	70.std(v2/v1)	88.var(tv1/tv2)	74.std(tv1/ta1)
	34.var(t1)	67.std(ta1)	20.std(tpi)
	25.std(A1)		
UDFS (20)	103.iqr(sig)	45.var(w_75)	15.mean(w_75)
	101.25% quantile	102.75% quantile	100.mad(sig)
	99.std(sig)	2.mean(amp of foot)	3.mean(x)
	9.mean(x/(tpi-t1))	11.mean(A2)	10.mean(A1)
	1.mean(sys amp)	106.signal_entropy(sig)	46.mean(v1)
	50.mean(a1)	52.mean(a2)	7.mean(t1/x)
	6.mean(tpp)	5.mean(tpi)	

TABLE 7: Top-ranked features using IlFS, mCFS and CFS based Feature Selection Algorithms

Algorithm	Best Selected Features		
IlFS (21)	32.var(amp of foot)	61.mean(tv2/ta2)	15.mean(w_75)
	65.std(tv2)	45.var(w_75)	8.mean(t1/tpi)
	6.mean(tpp)	96.maxratio	13.mean(w_25)
	44.var(w_50)	106.spectral_entropy	43.var(w_25)
	10.mean(A1)	11.mean(A2)	41.var(A2)
	50.mean(a1)	74.std(tv1/ta1)	105.kurtosis(sig
	9.mean(x/(tpi-t1))	86.var(v2/v1)	57.mean(ta1/ta2)
mCFS (24)	3.mean(x)	32.var(foot amp)	40.var(A1)
	41.var(A2)	11.mean(A2)	10.mean(A1)
	1.mean(sys amp)	2.mean(foot amp)	82.var(a1)
	33.var(x)	100.mad(sig)	46.mean(v1)
	57.mean(ta1/ta2)	47.mean(tv1)	50.mean(a1)
	49.mean(tv2)	99.std(sig)	51.mean(ta1)
	84.var(a2)	59.mean(tv1/ta2)	5.mean(tpi)
	61.mean(tv2/ta2)	6.mean(tpp)	38.var(t1/tpi)
CFS (14)	40.var(A1)	61.mean(tv2/ta2)	66.std(a1)
	8.mean(t1/tpi)	49.mean(tv2)	97.mean(sig)
	4.mean(t1)	32.var(amp of foot)	15.mean(w_75)
	45.var(w_75)	69.std(ta2)	6.mean(tpp)
	5.mean(tpi)	65.std(tv2)	

This article has been accepted for publication in a future issue of this journal, but has not been fully edited. Content may change prior to final publication. Citation information: DOI 10.1109/ACCESS.2021.3095380, IEEE Access

sets of features that circumvent the combinatorial issue [58]. **Table 7**, shows the top-ranked 21 features among which 14 were from the PPG signal and 5 derivative and 2 statistical features are also contributed in top 21.

Multi cluster feature selection (mCFS): mCFS requires a sparse eigen problem and an L1- regularized least squares question to efficiently solve the corresponding optimization problem [59]. Top-ranked 24 features were identified where 12 are PPG signal features, 10 derivative and 2 statistical features were mostly contributed in the top 24.

Correlation based feature selection (CFS): CFS is an embedded process that selects features in a sequential backward exclusion fashion to rank top features using linear SVM [60]. In **Table 7**, the most contributory features are 14 of the 107 features and 8 of the 15 features contributed only on the PPG signal. And rest of the 5 are the derivative and 1 from statistical features.

E. MACHINE LEARNING

Training, validation, and testing of the machine learning models were performed using 5-fold cross-validation. **Table 8** summarizes the number of PPG signal segments were used for training, validation, and testing. 80% of 758 recordings were used for training while 20% out of training samples were used for validation and 20% of 758 recordings were used for testing. We then extracted the features. Regression Learner App of MATLAB 2019b [61] was used to estimate respiration rate (RR). Five different algorithms (Support Vector Regression (SVR), Gaussian Process Regression (GPR), Ensemble Trees Linear Regression, and Regression Trees) with 19 different variations were evaluated. Furthermore, Artificial Neural Network (ANN), and Generalized Regression Neural Network (GRNN) were also investigated.

TABLE 8: Description of train, validation, and test set

Train set	Validation set	Test set
486	121	151

Gaussian Process Regression (GPR): GPR is a Bayesian regression approach, which works well on small datasets. Where most of the supervised machine learning algorithms learn the exact values of the function for each parameter, GPR learns a distribution of probability over all possible values [62].

Ensemble Trees: In this algorithm, multiple regression trees are combined using a weighted combination. The main idea behind this type of model is to use the strength of multiple weak learners to create a strong learner [63].

Support Vector Regression (SVR): It is a supervised learning algorithm where SVR is trained using the symmetrical loss function that punishes both higher and lower misprediction [64].

Artificial Neural Network (ANN): ANN tries to understand the relations between a set of data in a way that mimics the process of human brain behavior. It uses a set of interconnected artificial neurons in the layered structure and ANN can work very well on different types of data using this layered structure [65].

Generalized Regression Neural Network (GRNN): GRNN is a special type of neural network architecture where it has a radial basis layer and a special linear layer [66]. The uniqueness of GRNN is that it does not require a repeated training procedure like back-propagation networks compared to ANN where back-propagation is vital.

F. HYPERPARAMETER OPTIMIZATION

Initial training of machine learning algorithms was carried out using the default parameters of Regression Learner App of MATLAB 2019b [61]. The performance of these machine learning algorithms can be increased by tuning or optimization of the hyper-parameters of the algorithm. Bayesian Optimization was used in this work which was tuned for 30 iterations.

G. EVALUATION CRITERIA

In this study, five performance matrices were used. Here, X_p is the data that was predicted while X is the ground truth data and n denotes the number of samples or recordings.

I) Mean Absolute Error (MAE): The Mean Absolute Error is the mean of the absolute of the predicted errors.

$$MAE = \frac{1}{n}\sum_{n}|X_p - X| \tag{2}$$

II) Root Mean Squared Error (RMSE): RMSE measures the standard deviation of the prediction error or residuals, where residuals measure the distance of data points from the regression line. Therefore, RMSE is a way of measuring the spread of residuals, and the smaller the spread, the better the model.

$$RMSE = \sqrt{\frac{\sum|X_p - X|^2}{n}} \tag{3}$$

III) Correlation Co-efficient (R): R is used to measure how closely two variables (prediction and ground truth) are related. It is a statistical technique that also tells us how close the prediction matches with the ground truth.

$$R = \sqrt{1 - \frac{MSE(Model)}{MSE(Baseline)}} \tag{4}$$

$$where\ MSE(Baseline) = \frac{\sum|X - mean(X)|}{n}$$

IV) 2SD : Standard deviation(SD) is a statistical technique that measures the spread of data relative to its mean. It is calculated by computing the square root of the variance. 2SD is the double of SD. 2SD is important because it represents the 95% confidence interval.

$$2SD = 2\times SD = 2\times\sqrt{\frac{\sum(error - mean(error))^2}{n}} \tag{5}$$

$$where\ error = X_p - X$$

This article has been accepted for publication in a future issue of this journal, but has not been fully edited. Content may change prior to final publication. Citation information: DOI 10.1109/ACCESS.2021.3095380, IEEE Access

V) Limit of Agreement(LOA):Limit of agreement calculates the interval in which a percentage of the differences between two measurements (prediction and ground truth) lie. LOA captures both random (precision) and systematic (bias). It is therefore a useful way of measuring the performance of ML models. 95% LOA were computed in this study.

Among these criteria, RMSE and 2SD were chosen as the main criteria based on the reporting in the literature [22]–[24], [26].

III. RESULTS AND DISCUSSION

This section describes the evaluation results of the different machine learning algorithms used in this work. Out of the 19 classical machine learning algorithms evaluated in this study, SVR, GPR, and Ensemble trees were outperformers.

TABLE 9: Comparative performance of different machine learning models with different feature selection techniques

Algorithm	Metric	GPR	SVR	Ensemble
All Features	RMSE	2.92	3.14	3.38
	2SD	5.89	6.30	6.67
Relieff	RMSE	2.85	3.17	3.61
	2SD	5.70	6.33	7.12
Laplacian	RMSE	3.95	4.12	4.38
	2SD	7.88	8.25	8.57
mCFS	RMSE	2.88	3.18	3.75
	2SD	5.73	6.29	7.31
UDFS	RMSE	3.35	3.74	4.09
	2SD	6.70	7.37	8.03
Llcfs	RMSE	3.13	3.57	3.98
	2SD	6.26	7.04	7.74
CFS	RMSE	3.27	3.68	4.12
	2SD	6.49	7.22	8.01
Fsasl	RMSE	3.26	3.56	4.07
	2SD	6.49	7.03	7.96
Ufsol	RMSE	3.82	3.94	4.58
	2SD	7.64	8.04	9.36
Lasso	RMSE	3.05	3.30	3.80
	2SD	6.21	6.53	7.50
Fitrgp	RMSE	**2.66**	**2.96**	**3.57**
	2SD	**5.30**	**5.90**	**7.02**

In **Table 9**, it can be seen that the features selected by the Fitrgp technique were outperforming for different algorithms (SVR, GPR, and Ensemble Trees). This feature selection algorithm produced the best results for each ML model. However, the GPR model in combination with the Fitrgp feature selection technique provides superior performance with the state-of-the-art RMSE and 2SD of 2.66 and 5.30, respectively.

Since it has been observed in **Table 9** that GPR performed the best among all classical machine learning techniques tested in this work, the hyper-parameter optimization performance of GPR was compared with ANN and GRNN. The process can be seen in **Figure 8**. The best model having a Sigma of 4.318, a linear basis function, an isotropic exponential kernel function and a kernel scale of 0.54439.

The comparative performance of ANN, GRNN, and optimized GPR is shown in **Table 10**. It can be seen that the Fitrgp is outperforming the rest of the feature selection techniques. Among the machine learning algorithms, the optimized GPR marginally outperforms GRNN while performing significantly better than ANN. Therefore, the optimized GPR model was selected as the best performing model in this work.

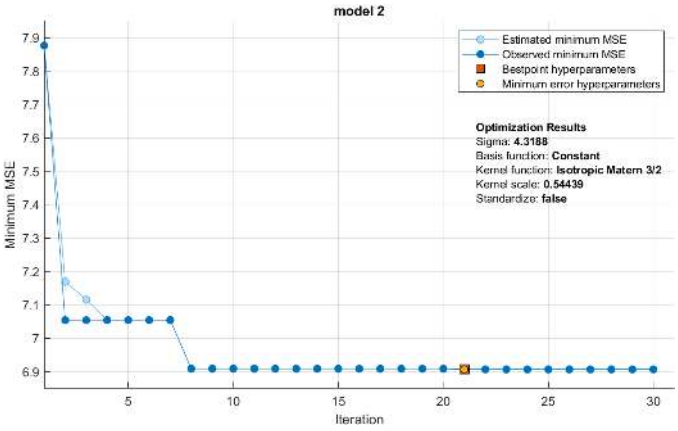

FIGURE 8: Hyperparameter Optimization of GPR model.

TABLE 10: Performance comparison of optimized machine learning models using different feature selection techniques

Algorithm	Metric	Optimized GPR	ANN	GRNN
All Features	RMSE	3.07	4.93	3.67
	2SD	6.09	9.81	6.92
Relieff	RMSE	2.83	4.07	3.28
	2SD	5.73	8.42	6.67
Laplacian	RMSE	3.47	5.66	4.39
	2SD	7.90	11.27	8.74
mCFS	RMSE	2.81	4.53	3.09
	2SD	5.70	9.03	6.14
UDFS	RMSE	3.34	4.50	3.59
	2SD	6.52	8.98	7.17
Llcfs	RMSE	3.10	4.51	3.85
	2SD	6.20	9.09	7.07
CFS	RMSE	3.17	5.09	3.67
	2SD	6.39	10.15	7.29
Fsasl	RMSE	3.16	5.39	3.69
	2SD	6.01	10.15	7.34
Ufsol	RMSE	3.84	5.24	4.21
	2SD	7.65	10.47	8.41
Lasso	RMSE	2.72	4.77	3.46
	2SD	5.45	9.42	6.83
Fitrgp	RMSE	**2.63**	**4.05**	**2.84**
	2SD	**5.26**	**8.08**	**5.68**

Figure 9, shows the best performing GPR model with and without the use of the feature selection algorithm. The result is visualized using regression and a Bland-Altman plot. The regression plot allows seeing how close the predictions are to the ground truth with the help of a trendline. The closer the trendline is to the $y = x$ line, the better the model. Bland-Altman plot allows us to see the spread of the data and also allows us to see the 95% limit of agreement (LOA) of the data, where a smaller LOA means a better model. **Figure 9**, shows that with all features, the algorithm had an R-value of 0.857 and an LOA of -5.82 to 5.67 bpm. With the feature selection algorithm (Fitrgp), the R-value is increased to 0.883 and the LOA reduces to -5.16 to 5.28 bpm.

This article has been accepted for publication in a future issue of this journal, but has not been fully edited. Content may change prior to final publication. Citation information: DOI 10.1109/ACCESS.2021.3095380, IEEE Access

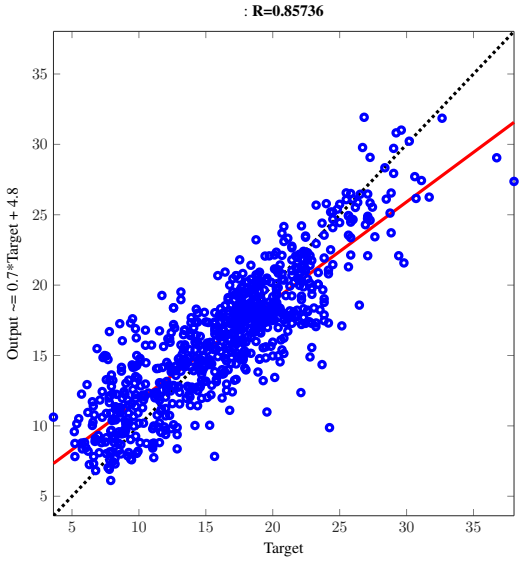

(a) All features Regression Plot

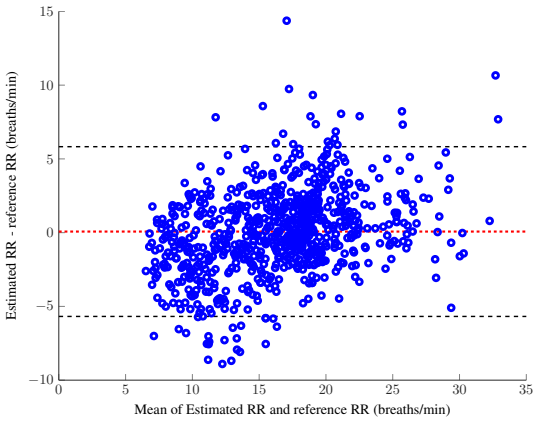

(b) All features Bland-Altman Plot

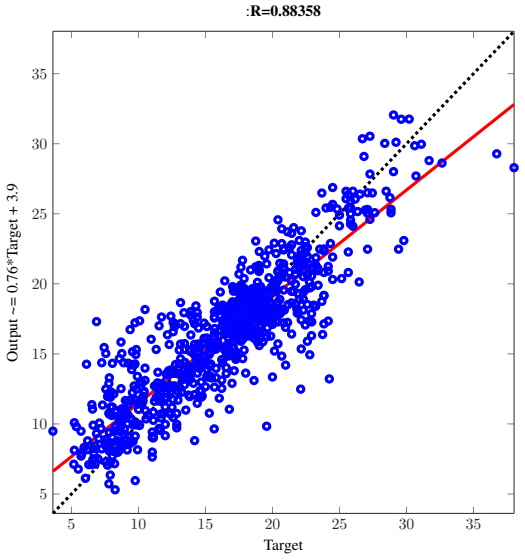

(c) Fitrgp based features Regression Plot

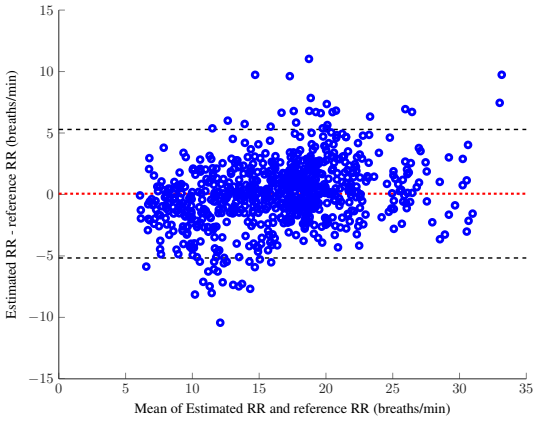

(d) Fitrgp based features Bland-Altman Plot

FIGURE 9: GPR model with Regression and Bland-Altman plot (a-b) for all features and (c-d) for Fitrgp based features.

The effect of hyperparameter optimization of the GPR model is shown in **Figure 10**. When comparing both the optimized models, it can be seen that the model with no feature selection had an R-value of 0.841 and an LOA of -5.83 to 6.26 bpm while the optimized GPR model with feature selection provides an R-value of 0.885 and the LOA of -5.16 to 5.25 bpm. Hence, it can be concluded that the feature selection algorithm helps in increasing the performance of the GPR model. Comparing **Figures 9** and **10**, it can be noticed that hyperparameter tuning has helped only feture selection model. However, the best performance can be observed with the optimized GPR along with the Fitrgp feature selection algorithm. Several factors made it difficult to compare the reported performance of algorithms of different research groups in the literature, such as the use of different statistical tests, data from different subject groups, and the lack of consistent algorithm implementations. As a result, it is not possible to decide from the literature which algorithms score higher. A comprehensive comparison of RR estimation is summarized with the state-of-the-art literatures in **Table 11**. As shown in **Table 11** Motin et al. [27] introduced a novel approach to the continuous control of PPG-based RR estimation using a smart fusion strategy based on EEMD is one of the best performing approaches. Estimating RR under daily living conditions is challenging, as the PPG signal is affected by the motion artifacts. The median absolute error (MAE) in [27].

L'Her et al. [29] described the accuracy of measurements of the respiratory rate using a specially developed reflex-

This article has been accepted for publication in a future issue of this journal, but has not been fully edited. Content may change prior to final publication. Citation information: DOI 10.1109/ACCESS.2021.3095380, IEEE Access

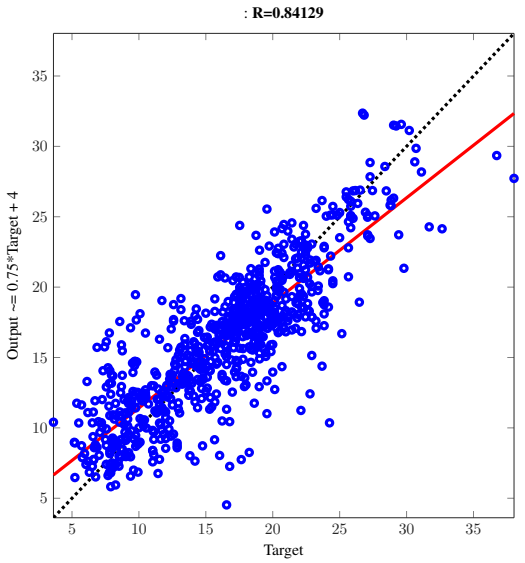

(a) All features Regression Plot

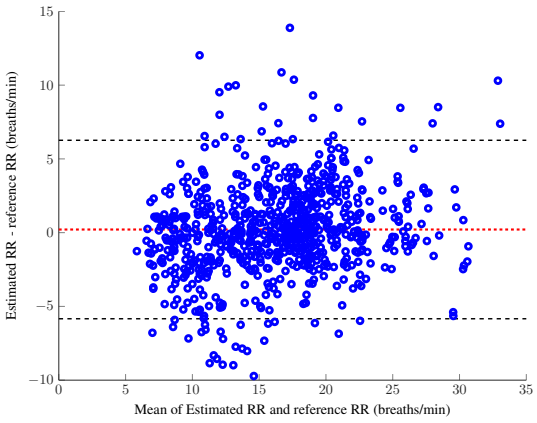

(b) All features Bland-Altman Plot

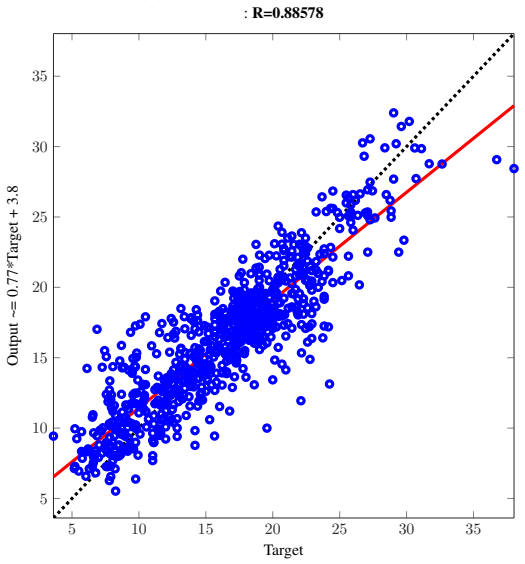

(c) Fitrgp based features Regression Plot

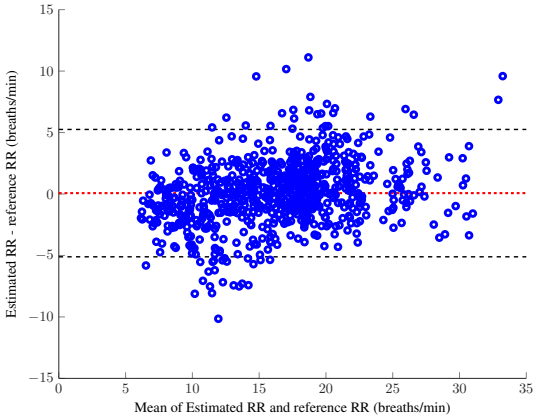

(d) Fitrgp based features Bland-Altman Plot

FIGURE 10: Optimized GPR model with Regression and Bland-Altman plot (a-b) for all features and (c-d) for Fitrgp based features.

mode photoplethysmographic pathological signal analysis (PPG-RR) and validated its implementation within medical devices. They experimented with this on 30 intensive care unit (ICU) patients where a correlation coefficient for RR of 0.78 was achieved. Motin et al. [28] used the EMD family and PCA-based hybrid model to remove RR from PPG, a natural extension of their previously built hybrid PCA-EMD (EEMD) system. The MAE for the model tested on MIMIC datasets of 53 subjects were varied from 0 to 5.03 bpm.

With the assistance of Time Frequency (TF) reassignments and a particle filter, Pirhonen et al. [30] suggested the use of amplitude fluctuations of the PPG signals to approximate RR. Vortal database was used in that study. The highest results were achieved using wavelet synchrosqueezing transform, which produced an MAE and RMSE of 2.33 and 3.68 bpm, respectively.

Jarchi et al. [31] presented a case study on 10 subjects to estimate RR from the PPG signals relative to accelerometer and achieved an MAE of 2.56 bpm. Zhang et al. [26], [43] proposed the estimation of the RR from the PPG signal using joint sparse signal reconstruction (JSSR) and Spectra Fusion (SF) from 42 subjects and achieved an LOA and RMSE of -5.58 to 4.88, 2.81 and -6.24 to 5.45, 3.25 bpm, respectively. Pimentel et al. [37] estimated RR using autoregressive model from two publically available database, where they achieved an comparable MAE of 4.0 (0.3-3.3) and 1.5 (1.8-5.5) for a

This article has been accepted for publication in a future issue of this journal, but has not been fully edited. Content may change prior to final publication. Citation information: DOI 10.1109/ACCESS.2021.3095380, IEEE Access

TABLE 11: Comparison of the proposed method with the recent related works concerning the database, methodology, and estimation error

Author	Year	Database	Subject	Method	Metric	Result
Motin et al. [27]	2020	Own Database	10 Subjects	Empirical Mode Decom-position	MAE RMSE R 2SD LOA	3.05 - - - -
L'Her et al. [29]	2019	Own Database	30 ICU Patient	Own Approach	MAE RMSE R 2SD LOA	- - 0.78 - -
Motin et al. [28]	2019	MIMIC Database	53 Subjects	Empirical Mode Decom-position	MAE RMSE R 2SD LOA	0 - 5.03 - - - -
Jarch et al. [31]	2018	BIDMC Dataset	10 Subjects	Accelero-meter	MAE RMSE R 2SD LOA	2.56 - - - -
Pirhonen et al. [30]	2018	Vortal Database	39 Subjects	Wavelet Synchro-squeezing Transform	MAE RMSE R 2SD LOA	2.33 3.68 - - -
Zhang et al. [26]	2017	Capnobase Dataset	42 Subjects	Joint sparse signal Reconstr-action	MAE RMSE R 2SD LOA	- 2.89 - - -5.6 to 4.9
Zhang et al. [43]	2016	Capnobase Dataset	42 Subjects	Joint sparse signal Reconstr-action	MAE RMSE R 2SD LOA	- 3.25 - - -6.24 to 5.45
Pimentel et al. [37]	2016	BIDMC Dataset	53 Subjects	Autoregressive-model	MAE RMSE R 2SD LOA	4.0 (0.3-3.3) - - - -
Pimentel et al. [37]	2016	Capnobase Dataset	42 Subjects	Autoregressive-model	MAE RMSE R 2SD LOA	1.5 (1.8-5.5) - - - -
Charlton et al. [23]	2016	Vortal Dataset	39 Subjects	92 Different Algorithm	MAE RMSE R 2SD LOA	- - - 6.20 -5.2 to 7.2
This Work	2021	Vortal Database	39 Subjects	Machine Learning	MAE RMSE R 2SD LOA	**1.97** **2.63** **0.88** **5.25** **-5.16 to 5.25**

windows size of 32 second. But one of their limitation was, they discarded 36% of windows due to motion artifact effect. Charlton et al. [23] divided the algorithm into three phases: respiratory signal extraction, RR estimation, and estimation fusion and 314 different algorithms were assessed and the best algorithm had 95 percent LOA and 2SD of -5.1 to 7.2, and 6.2 bpm, respectively.

There is no exact medical standard regarding the estimation of RR. However, in a review paper [22] where over 196 traditional RR extraction technique were reviewed, they stated that an MAE less than 2 bpm should provide a suitable indicator for a good estimator. The machine learning model suggested in this analysis was measured with much higher precision and accuracy which shown in **Table 11**.

The computational complexity reduction mentioned in the paper is due to the usage of feature optimization and ma-

chine learning technique which reduces the computational complexity of the estimation system while make the system robust for motion-corrupted PPG signal. On the other hand, traditional approach [23], [24] extracts respiratory signal from PPG signals using amplitude modulation (AM), frequency modulation (FM) and baseline wandering. This estimation only works with motion-free PPG signals to estimate respiratory rate. In the proposed system, the inference time for estimating PPG depends on VMD and feature extraction techniques but the regression process is quite fast while other approaches fails on the motion corrupted PPG signals even though these might be faster than ML based approach. Since the respiration is a slow changing signal, we believe ML model can work in real-time if deployed in the mobile devices or smart watches. our approach is computationally expensive but reliable and robust now.

IV. LIMITATIONS

The key limitation of this study is that the VORTAL dataset was collected from the young healthy subjects at rest. In our future work, we are aiming to estimate respiratory rates from patients with different age groups and with different clinical conditions.

V. CONCLUSIONS

In this study, the authors proposed and developed a machine learning-based method for predicting RR from the PPG signal features. This successfully shows how the motion artifact corrected PPG signal can be used to correctly estimate the RR value invasively. The entire prepossessing process of the PPG signals to extract the features, feature selection, and training of the algorithms were discussed. The method used 107 time-domain, frequency-domain, and statistical features to extract meaningful information from the PPG signal. ANN and GRNN and 19 other machine learning models were trained, validated, and tested for RR estimation, where the performance of GPR, SVR, ensemble trees, ANN and GRNN were promising. To reduce computational complexity and the risk of over-fitting, different feature selection algorithms were investigated. It was observed that a combination of Fitrgp feature selection and GPR machine-learning algorithm produced the best result. However, hyper-parameter optimization can improve the model performance further. The fine-tuned model provides an RMSE, MAE, R, and 2SD score of 2.63, 1.97, 0.88, and 5.25 bpm for the estimation of RR. This state-of-the-art performance of the proposed model will make it possible to deploy this for ambulatory and intensive care units as well for remote health care monitoring.

ACKNOWLEDGEMENT

This work was made possible by NPRP12S-0227-190164 from the Qatar National Research Fund, a member of Qatar Foundation, a member of Qatar Foundation, Doha, Qatar. Open Access funding provided by the Qatar National Library. The statements made herein are solely the responsibility of the authors.

REFERENCES

[1] John F Fieselmann, Michael S Hendryx, Charles M Helms, and Douglas S Wakefield. Respiratory rate predicts cardiopulmonary arrest for internal medicine inpatients. Journal of general internal medicine, 8(7):354–360, 1993.

[2] DR Goldhill, SA White, and A Sumner. Physiological values and procedures in the 24 h before icu admission from the ward. Anaesthesia, 54(6):529–534, 1999.

[3] Mark H Ebell. Predicting pneumonia in adults with respiratory illness. American family physician, 76(4):560, 2007.

[4] Michelle Cretikos, Jack Chen, Ken Hillman, Rinaldo Bellomo, Simon Finfer, Arthas Flabouris, Merit Study Investigators, et al. The objective medical emergency team activation criteria: a case–control study. Resuscitation, 73(1):62–72, 2007.

[5] Thomas R Gravelyn and John G Weg. Respiratory rate as an indicator of acute respiratory dysfunction. Jama, 244(10):1123–1125, 1980.

[6] Roland MH Schein, Nelson Hazday, Maria Pena, Bradley H Ruben, and Charles L Sprung. Clinical antecedents to in-hospital cardiopulmonary arrest. Chest, 98(6):1388–1392, 1990.

[7] RW Duckitt, R Buxton-Thomas, J Walker, E Cheek, V Bewick, R Venn, and LG Forni. Worthing physiological scoring system: derivation and validation of a physiological early-warning system for medical admissions. an observational, population-based single-centre study. British journal of anaesthesia, 98(6):769–774, 2007.

[8] B William, G Albert, C Ball, D Bell, R Binks, L Durham, J Eddleston, N Edwards, D Evans, M Jones, et al. National early warning score (news): Standardizing the assessment of acute illness severity in the nhs. Report of a Working Party, 2012.

[9] Nasim Farrohknia, Maaret Castrén, Anna Ehrenberg, Lars Lind, Sven Oredsson, Håkan Jonsson, Kjell Asplund, and Katarina E Göransson. Emergency department triage scales and their components: a systematic review of the scientific evidence. Scandinavian journal of trauma, resuscitation and emergency medicine, 19(1):42, 2011.

[10] Walter Karlen, Srinivas Raman, J Mark Ansermino, and Guy A Dumont. Multiparameter respiratory rate estimation from the photoplethysmogram. IEEE Transactions on Biomedical Engineering, 60(7):1946–1953, 2013.

[11] Ambreen Khalil, Gabor Kelen, and Richard E Rothman. A simple screening tool for identification of community-acquired pneumonia in an inner city emergency department. Emergency Medicine Journal, 24(5):336–338, 2007.

[12] Marco AF Pimentel, Peter H Charlton, and David A Clifton. Probabilistic estimation of respiratory rate from wearable sensors. In Wearable electronics sensors, pages 241–262. Springer, 2015.

[13] Samuel Z Goldhaber, Luigi Visani, Marisa De Rosa, et al. Acute pulmonary embolism: clinical outcomes in the international cooperative pulmonary embolism registry (icoper). The Lancet, 353(9162):1386–1389, 1999.

[14] Michelle A Cretikos, Rinaldo Bellomo, Ken Hillman, Jack Chen, Simon Finfer, and Arthas Flabouris. Respiratory rate: the neglected vital sign. Medical Journal of Australia, 188(11):657–659, 2008.

[15] Paris B Lovett, Jason M Buchwald, Kai Stürmann, and Polly Bijur. The vexatious vital: neither clinical measurements by nurses nor an electronic monitor provides accurate measurements of respiratory rate in triage. Annals of emergency medicine, 45(1):68–76, 2005.

[16] Keir EJ Philip, Emma Pack, Valentina Cambiano, Hannah Rollmann, Simon Weil, and James O'Beirne. The accuracy of respiratory rate assessment by doctors in a london teaching hospital: a cross-sectional study. Journal of clinical monitoring and computing, 29(4):455–460, 2015.

[17] Michael B Jaffe. Infrared measurement of carbon dioxide in the human breath:"breathe-through" devices from tyndall to the present day. Anesthesia & Analgesia, 107(3):890–904, 2008.

[18] George B Moody, Roger G Mark, Andrea Zoccola, and Sara Mantero. Derivation of respiratory signals from multi-lead ecgs. Computers in cardiology, 12(1985):113–116, 1985.

[19] Christina Orphanidou, Susannah Fleming, Syed Ahmar Shah, and Lionel Tarassenko. Data fusion for estimating respiratory rate from a single-lead ecg. Biomedical Signal Processing and Control, 8(1):98–105, 2013.

[20] Leila Mirmohamadsadeghi and Jean-Marc Vesin. Respiratory rate estimation from the ecg using an instantaneous frequency tracking algorithm. Biomedical Signal Processing and Control, 14:66–72, 2014.

[21] Barbara J Drew, Patricia Harris, Jessica K Zègre-Hemsey, Tina Mammone, Daniel Schindler, Rebeca Salas-Boni, Yong Bai, Adelita Tinoco, Quan Ding, and Xiao Hu. Insights into the problem of alarm fatigue with physiologic monitor devices: a comprehensive observational study of consecutive intensive care unit patients. PloS one, 9(10):e110274, 2014.

[22] Peter H Charlton, Drew A Birrenkott, Timothy Bonnici, Marco AF Pimentel, Alistair EW Johnson, Jordi Alastruey, Lionel Tarassenko, Peter J Watkinson, Richard Beale, and David A Clifton. Breathing rate estimation from the electrocardiogram and photoplethysmogram: A review. IEEE reviews in biomedical engineering, 11:2–20, 2017.

[23] Peter H Charlton, Timothy Bonnici, Lionel Tarassenko, David A Clifton, Richard Beale, and Peter J Watkinson. An assessment of algorithms to estimate respiratory rate from the electrocardiogram and photoplethysmogram. Physiological measurement, 37(4):610, 2016.

[24] Peter H Charlton, Timothy Bonnici, Lionel Tarassenko, Jordi Alastruey, David A Clifton, Richard Beale, and Peter J Watkinson. Extraction of respiratory signals from the electrocardiogram and photoplethysmogram: technical and physiological determinants. Physiological measurement, 38(5):669, 2017.

[25] Syed Ahmar Shah, Susannah Fleming, Matthew Thompson, and Lionel Tarassenko. Respiratory rate estimation during triage of children in hospitals. Journal of medical engineering & technology, 39(8):514–524, 2015.

[26] Xiaorong Zhang and Quan Ding. Respiratory rate estimation from the photoplethysmogram via joint sparse signal reconstruction and spectra fusion. Biomedical Signal Processing and Control, 35:1–7, 2017.

[27] Mohammod Abdul Motin, Chandan Kumar Karmakar, Dinesh Kant Kumar, and Marimuthu Palaniswami. Ppg derived respiratory rate estimation in daily living conditions. In 2020 42nd Annual International Conference of the IEEE Engineering in Medicine & Biology Society (EMBC), pages 2736–2739. IEEE, 2020.

[28] Mohammod Abdul Motin, Chandan Kumar Karmakar, and Marimuthu Palaniswami. Selection of empirical mode decomposition techniques for extracting breathing rate from ppg. IEEE Signal Processing Letters, 26(4):592–596, 2019.

[29] Erwan L'Her, Quang-Thang N'Guyen, Victoire Pateau, Laetitia Bodenes, and François Lellouche. Photoplethysmographic determination of the respiratory rate in acutely ill patients: validation of a new algorithm and implementation into a biomedical device. Annals of intensive care, 9(1):11, 2019.

[30] Mikko Pirhonen, Mikko Peltokangas, and Antti Vehkaoja. Acquiring respiration rate from photoplethysmographic signal by recursive bayesian tracking of intrinsic modes in time-frequency spectra. Sensors, 18(6):1693, 2018.

[31] Delaram Jarchi, Sarah J Rodgers, Lionel Tarassenko, and David A Clifton. Accelerometry-based estimation of respiratory rate for post-intensive care patient monitoring. IEEE Sensors Journal, 18(12):4981–4989, 2018.

[32] Vera Hartmann, Haipeng Liu, Fei Chen, Wentao Hong, Stephen Hughes, and Dingchang Zheng. Towards accurate extraction of respiratory frequency from the photoplethysmogram: Effect of measurement site. Frontiers in physiology, 10:732, 2019.

[33] Duncan Luguern, Simon Perche, Yannick Benezeth, Virginie Moser, L Andrea Dunbar, Fabian Braun, Alia Lemkaddem, Keisuke Nakamura, Randy Gomez, and Julien Dubois. An assessment of algorithms to estimate respiratory rate from the remote photoplethysmogram. In Proceedings of the IEEE/CVF Conference on Computer Vision and Pattern Recognition Workshops, pages 304–305, 2020.

[34] Moajjem Hossain Chowdhury, Md Nazmul Islam Shuzan, Muhammad EH Chowdhury, Zaid B Mahbub, M Monir Uddin, Amith Khandakar, and Mamun Bin Ibne Reaz. Estimating blood pressure from the photoplethysmogram signal and demographic features using machine learning techniques. Sensors, 20(11):3127, 2020.

[35] Muhammad EH Chowdhury, Amith Khandakar, Khawla Alzoubi, Samar Mansoor, Anas M Tahir, Mamun Bin Ibne Reaz, and Nasser Al-Emadi. Real-time smart-digital stethoscope system for heart diseases monitoring. Sensors, 19(12):2781, 2019.

[36] Muhammad EH Chowdhury, Khawla Alzoubi, Amith Khandakar, Ridab Khallifa, Rayaan Abouhasera, Sirine Koubaa, Rashid Ahmed, and Anwarul Hasan. Wearable real-time heart attack detection and warning system to reduce road accidents. Sensors, 19(12):2780, 2019.

[37] Marco AF Pimentel, Alistair EW Johnson, Peter H Charlton, Drew Birrenkott, Peter J Watkinson, Lionel Tarassenko, and David A Clifton. Toward a robust estimation of respiratory rate from pulse oximeters. IEEE Transactions on Biomedical Engineering, 64(8):1914–1923, 2016.

[38] Yue-Der Lin, Ya-Hsueh Chien, and Yi-Sheng Chen. Wavelet-based embedded algorithm for respiratory rate estimation from ppg signal. Biomedical Signal Processing and Control, 36:138–145, 2017.

[39] Susannah G Fleming and Lionel Tarassenko. A comparison of signal processing techniques for the extraction of breathing rate from the photoplethysmogram. Int. J. Biol. Med. Sci, 2(4):232–236, 2007.

[40] Yongjin Zhou, Yongping Zheng, Congzhi Wang, and Junfeng Yuan. Extraction of respiratory activity from photoplethysmographic signals based on an independent component analysis technique: Preliminary report. Instrumentation Science and Technology, 34(5):537–545, 2006.

[41] Silvia Moreno, Andres Quintero-Parra, Carlos Ochoa-Pertuz, Reynaldo Villarreal, and Isaac Kuzmar. A signal processing method for respiratory rate estimation through photoplethysmography. International Journal of Signal Processing, Image Processing and Pattern Recognition, 11(2):1–10, 2018.

[42] Lena Nilsson, Anders Johansson, and Sigga Kalman. Monitoring of respiratory rate in postoperative care using a new photoplethysmographic technique. Journal of clinical monitoring and computing, 16(4):309–315, 2000.

[43] Xiaorong Zhang and Quan Ding. Respiratory rate monitoring from the photoplethysmogram via sparse signal reconstruction. Physiological measurement, 37(7):1105, 2016.

[44] K Venu Madhav, M Raghu Ram, E Hari Krishna, Nagarjuna Reddy Komalla, and K Ashoka Reddy. Robust extraction of respiratory activity from ppg signals using modified mspca. IEEE Transactions on Instrumentation and Measurement, 62(5):1094–1106, 2013.

[45] Ayan Chatterjee and Uttam Kumar Roy. Ppg based heart rate algorithm improvement with butterworth iir filter and savitzky-golay fir filter. In 2018 2nd International Conference on Electronics, Materials Engineering & Nano-Technology (IEMENTech), pages 1–6. IEEE, 2018.

[46] Yanxue Wang and Richard Markert. Filter bank property of variational mode decomposition and its applications. Signal Processing, 120:509–521, 2016.

[47] Biplab Roy, Rajarshi Gupta, and Jayanta K Chandra. Estimation of respiration rate from motion corrupted photoplethysmogram: A combined time and frequency domain approach. In 2019 IEEE Region 10 Symposium (TENSYMP), pages 292–297. IEEE, 2019.

[48] Giorgio Roffo. Feature selection library (matlab toolbox). arXiv preprint arXiv:1607.01327, 2016.

[49] Carl Edward Rasmussen. Gaussian processes in machine learning. In Summer School on Machine Learning, pages 63–71. Springer, 2003.

[50] Jeffrey C Lagarias, James A Reeds, Margaret H Wright, and Paul E Wright. Convergence properties of the nelder–mead simplex method in low dimensions. SIAM Journal on optimization, 9(1):112–147, 1998.

[51] Huan Liu and Hiroshi Motoda. Computational methods of feature selection. CRC Press, 2007.

[52] Igor Kononenko, Edvard Šimec, and Marko Robnik-Šikonja. Overcoming the myopia of inductive learning algorithms with relieff. Applied Intelligence, 7(1):39–55, 1997.

[53] Marko Robnik-Šikonja and Igor Kononenko. Theoretical and empirical analysis of relieff and rrelieff. Machine learning, 53(1-2):23–69, 2003.

[54] Liang Du and Yi-Dong Shen. Unsupervised feature selection with adaptive structure learning. In Proceedings of the 21th ACM SIGKDD international conference on knowledge discovery and data mining, pages 209–218, 2015.

[55] Jun Guo, Yanqing Quo, Xiangwei Kong, and Ran He. Unsupervised feature selection with ordinal locality. In 2017 IEEE international conference on multimedia and expo (ICME), pages 1213–1218. IEEE, 2017.

[56] Xiaofei He, Deng Cai, and Partha Niyogi. Laplacian score for feature selection. In Advances in neural information processing systems, pages 507–514, 2006.

[57] Yi Yang, Heng Tao Shen, Zhigang Ma, Zi Huang, and Xiaofang Zhou. l 2, 1-norm regularized discriminative feature selection for unsupervised learning. In IJCAI international joint conference on artificial intelligence, 2011.

[58] Hong Zeng and Yiu-ming Cheung. Feature selection and kernel learning for local learning-based clustering. IEEE transactions on pattern analysis and machine intelligence, 33(8):1532–1547, 2010.

[59] Marco Cristani, Giorgio Roffo, Cristina Segalin, Loris Bazzani, Alessandro Vinciarelli, and Vittorio Murino. Conversationally-inspired stylometric features for authorship attribution in instant messaging. In Proceedings of the 20th ACM international conference on Multimedia, pages 1121–1124, 2012.

[60] Isabelle Guyon, Jason Weston, Stephen Barnhill, and Vladimir Vapnik. Gene selection for cancer classification using support vector machines. Machine learning, 46(1-3):389–422, 2002.
[61] Regression learner app. https://www.mathworks.com/help/stats/regression-learner-app.html, accessed on 25 November 2020.
[62] Gaussian process regression models. https://www.mathworks.com/help/stats/gaussian-process-regression-models.html, accessed on 25 November 2020.
[63] Framework for ensemble learning. https://www.mathworks.com/help/stats/framework-for-ensemble-learning.html, accessed on 25 November 2020.
[64] Support vector machine regression. https://www.mathworks.com/help/stats/support-vector-machine-regression.html, accessed on 25 November 2020.
[65] What is a neural network? https://www.mathworks.com/discovery/neural-network.html, accessed on 25 November 2020.
[66] Generalized regression neural networks. https://www.mathworks.com/help/deeplearning/ug/generalized-regression-neural-networks.html, accessed on 25 November 2020.